

Electrochemical *in situ* reaction cell for X-ray scattering, diffraction and spectroscopy

A. Braun,^{a*} S. Shrout,^{a,b} A. C. Fowlks,^{a,c} B. A. Osaisai,^{a,b} S. Seifert,^d E. Granlund^e and E. J. Cairns^{a,e}

^aEnvironmental Energy Technologies, Ernest Orlando Lawrence Berkeley National Laboratory, Berkeley, CA 94720, USA,

^bSchool of Engineering and Computer Science, San Francisco State University, 1600 Holloway Avenue, San Francisco, CA 94132, USA, ^cDepartment of Materials Science and Engineering, University of Michigan, Ann Arbor, MI 48109, USA,

^dChemistry Division, Argonne National Laboratory, 9700 South Cass Avenue, Argonne, IL 60439, USA, and ^eDepartment of Chemical Engineering, University of California, Berkeley, CA 94720, USA. E-mail: artur.braun@alumni.ethz.ch

A versatile electrochemical *in situ* reaction cell for long-term hard X-ray experiments on battery electrodes is described. Applications include the small-angle scattering, diffraction and absorption spectroscopy of lithium manganese oxide electrodes.

Keywords: lithium battery; electrochemistry; SAXS; X-ray spectroscopy; *in situ* cell.

1. Introduction

On-line monitoring of changes in materials undergoing chemical reactions is usually performed by using *in situ* reaction chambers. In the last two decades, countless X-ray *in situ* chambers have been designed for battery research applications. Since some of the battery electrode materials are very sensitive to corrosion in the ambient atmosphere, including in particular the alkaline metal-based systems such as lithium batteries, the sealing of the cells plays a very important role.

While many different cell designs have been successfully developed and tested for short-term experiments, only few have been reported that allow for experiments that extend over several days or even weeks. One research group has overcome many of the obstacles related to electrochemical *in situ* X-ray experiments by switching to energy-dispersive X-ray diffraction, that utilize rather high X-ray energies (Ronci *et al.*, 2001); other groups depend on *in situ* cells that were manufactured in an industrial plant (Richard *et al.*, 1997) and on a particular diffractometer type (Gérand *et al.*, 1999). Another *in situ* cell (Koetschau *et al.*, 1995) allowed for long-term experiments, but did not contain lithium metal counter electrodes. The McBreen group has performed *in situ* X-ray diffraction and absorption, but they measured the cathode of a high-rate industrial battery which could be studied in a short time (Balasubramanian *et al.*, 2001).

Charging and discharging reactions in batteries are pronouncedly limited by diffusion and may take hours. Since the structure of electrodes may be dependent upon the number of charge and discharge cycles, experiments often take as long as weeks or months.

When exposed to the ambient atmosphere, the lithium reacts with the nitrogen in the air to form lithium nitride or, with the humidity to form lithium hydroxide. Some of the electrolytes used in batteries may also form aggressive reaction products; for instance, LiPF₆ forms hydrofluoric acid when in contact with the ambient humidity.

These corrosive reactions are common in batteries and must be minimized by using proper sealing. Regular battery test cells which

are not used for *in situ* studies are usually very carefully designed to satisfy the strict sealing requirements and allow cycling experiments for several months.

In contrast, *in situ* cells need X-ray windows and thus are more prone to leakage. In some of them, leakage problems are overcome by extensive use of sealants, and those cells are often for one-time use only.

In this paper we present a convenient re-usable cell with beryllium X-ray windows and sealing rings. It allows charging and discharging of the battery for several days without noticeable traces of corrosion of the lithium metal.

The cell's design allows for it to be employed in the transmission mode at any hard X-ray source. In particular, the cell was tested at beamline 12-ID (Braun *et al.*, 2001) at BESSRC-CAT, Advanced Photon Source, Argonne, IL, USA, and at beamlines 2-1 and 2-3 at Stanford Synchrotron Radiation Laboratory, Menlo Park, CA, USA.

To the best of our knowledge, this is the first time that a single *in situ* electrochemical cell has been used for X-ray techniques so different in nature such as X-ray diffraction, spectroscopy and anomalous small-angle scattering.

2. Design of the *in situ* cell

The cell design and a photograph are shown in a panel in Fig. 1. A schematic drawing of the flat cylindrical cell is given in Fig. 1(a). The main support of the cell is a stainless steel disk (15 cm diameter) and a polypropylene (PP) disk (9 cm diameter), both of 5 mm thickness. With steel bolts (size M 5), both disks are held together and contain the electrode sample, an ion-conducting separator, the electrolyte and a lithium metal counter electrode. Sealing of the cell is necessary to prevent the electrolyte from drying out and to prevent the sample from chemical reactions with the ambient atmosphere. The zone between the steel disk and the PP disk is the sample compartment, which is sealed by three concentric BUNA O-rings which have different diameters. Corresponding O-ring grooves are provided in both disks. Fig. 1(b) shows a magnified view of the portion of the cell that contains the electrode assembly. Both disks have a port of 1 mm × 2.5 mm in their center to allow the X-ray beam to pass through the cell. The ports on either side of the cell are capped with a beryllium disk of thickness 380 μm. The interfaces between the beryllium disks and the steel disk and the PP disk, respectively, are also sealed with three small concentric BUNA O-rings. On either side, a 30 mm-diameter aluminium disk holds the beryllium disks in place. In their center, the aluminium disks have a 7 mm-diameter opening to allow the X-ray beam to pass through.

We have carried out a systematic study on how many O-rings are necessary to provide sufficient protection. One single O-ring was clearly insufficient for proper sealing as required here. We found that a set of three O-rings provides very good sealing and is still efficient and feasible in terms of cell machining.

The thicknesses of the disks and the width of the holes determine the aspect ratio which is necessary to cover a desired Q -range for wide-angle X-ray diffraction. In the present case, a 2θ -angle of about 45° at maximum was permitted which allowed resolution of the [111] Bragg reflection of LiMn₂O₄ at X-ray energies of around 6500 eV. By choosing higher energies, the entire diffractogram becomes compressed and will be resolved in the 2θ -angle of about 45°.

The Be foils are covered with 25 μm-thick Kapton tape to prevent contact with the corrosive electrolyte.

The working electrode is in direct contact with the steel disk to guarantee electrical contact. The PP disk has two feed-throughs for stainless steel bolts which serve as contacts to the lithium counter

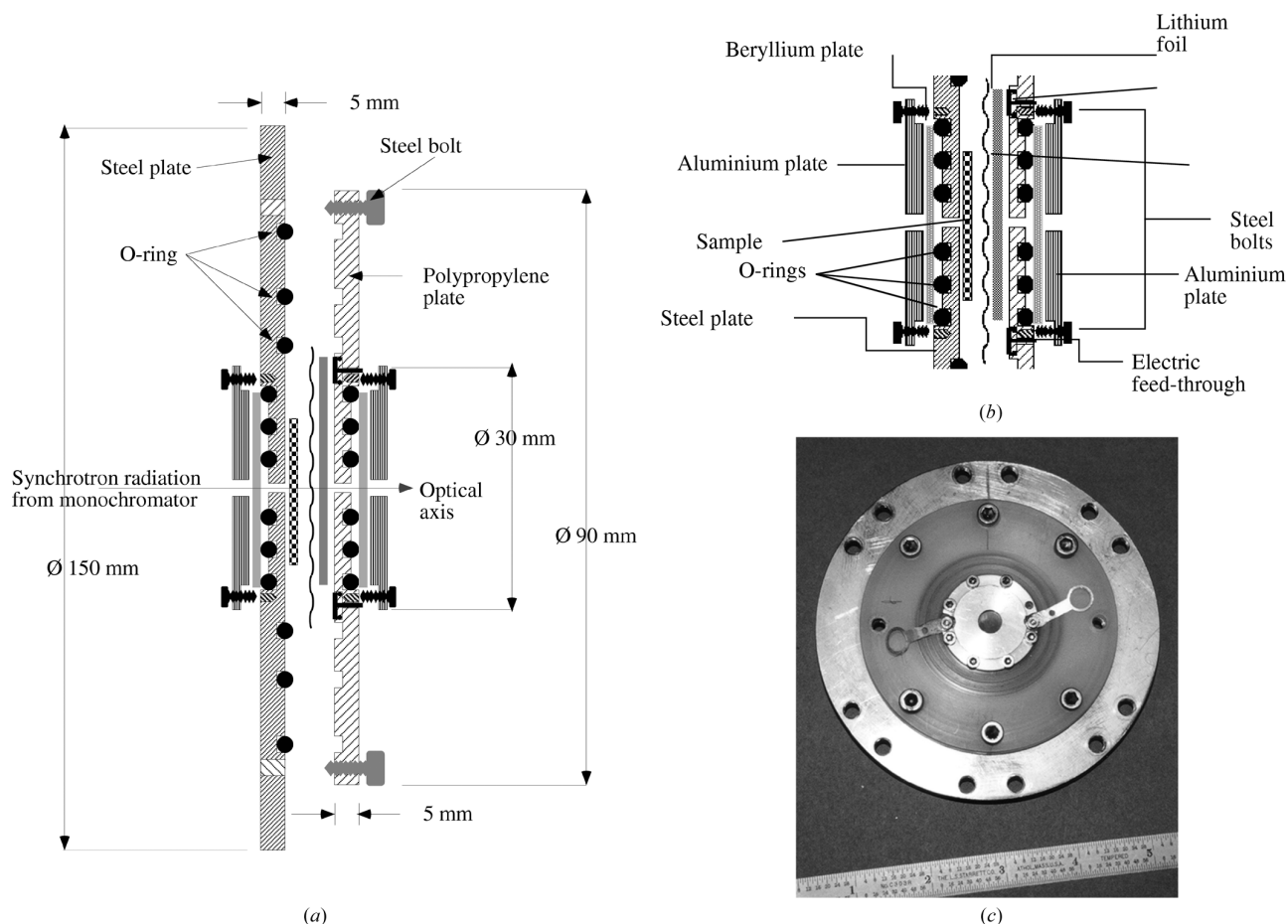


Figure 1

(a) Cross-sectional overview of the *in situ* cell. Not all of the parts refer to the same scale. (b) Magnified cross section of the central cell parts. (c) Photograph of the *in situ* cell, showing the PP disk on top of the stainless steel disk. The ruler shows the length scale in inches.

electrode and an optional reference electrode. Each of the two steel bolts is sealed with a tiny O-ring of diameter 2 mm; these seals are the least reliable parts in terms of contamination from the ambient atmosphere. After several days of operation, the side of the lithium foil which is next to the steel bolts exhibits typical traces of black lithium nitride, which is an indication that nitrogen has diffused around the O-ring. However, this effect was confined to an uncritical area of the cell.

Fig. 1(c) shows a photograph of the assembled cell with the PP disk on top of the steel disk. Two metal strips are contacted by the bolts in the feed-through for connection to the reference and counter electrodes. Numerous drilled holes in the metal disk allow for versatile mounting of the cell at the beamlines.

At SSRL and APS we assembled and sealed the cells in a portable helium-filled glove bag on site in their chemistry laboratories. On one occasion we assembled the cell in our home laboratory at LBNL and brought it to SSRL for experiments.

To enhance the sealing safety of the cell during experiments, we wrapped it in a conventional ziplock bag filled with helium. It turned out, however, that the cell remained fine without significant contamination or corrosion for more than four days without keeping it in helium.

3. Experimental

The first experimental results were obtained with a complete lithium manganese oxide cell. The LiMn_2O_4 spinel powder was synthesized

by mixing lithium carbonate Li_2CO_3 and manganese oxide MnO_2 (CMD IC#5, Japan Metals and Chemical) in the stoichiometric amounts and heating it in a muffle furnace with air at 1123 K and subsequent cooling.

The spinel powder was mixed with carbon (graphite from Timcal, and Shawinigan carbon black) and polymer binder (all together 5 wt%) and cast on an aluminium foil of thickness 25 μm , and subsequently sintered at 423 K, resulting in the positive electrode of thickness 40 μm , and containing spinel to about 95 wt%.

Electrodes with a diameter of 25 mm were punched from the foil sheet and vacuum dried for another 24 h, and then stored under argon before being used.

The positive electrode, with a polypropylene separator, electrolyte (LiPF_6 dissolved in dimethyl carbonate) and lithium foil (125 μm) as counter electrode was assembled to form the cell (Braun *et al.*, 2001).

The cell assembly was as follows:

All necessary cell parts, chemicals and tools for assembly were contained in either a helium-filled glove bag (for assembly at the synchrotron) or in an argon-filled glove box in our laboratory at LBNL. The beryllium windows were already assembled, and the O-rings already placed in the grooves. A piece of lithium foil, as large as the spinel electrode, was punched out from fresh supplies and squeezed onto the steel contact bolt of the PP disk; this made the counter electrode. Then, one single spinel/alu-foil assembly electrode was placed in the center of the steel disk, with the spinel side facing up, and the separator put on top of it. A small strip of lithium foil was placed on the separator such that it would later match the position of

critical balance of parameters that affect phase changes and phase purity in lithium manganese oxides is a topic that currently receives much attention from many research groups (Mishra *et al.*, 1999; Kanno *et al.*, 1999, and references therein).

When we plot the two diffractograms, obtained at 6500 and 6538 eV, in the classical way *versus* the 2Θ -angle, the latter diffractogram will be shifted towards smaller angles. We can compensate for this effect by using the scattering vector Q instead,

$$Q = (2 \sin \Theta)/\lambda.$$

The X-ray wavelength λ is related to the X-ray energy E via $E = hc/\lambda$.

Yet, we see in Fig. 4 that corresponding Bragg reflections are shifted, even if we plot them *versus* the scattering vector Q . Thus, the shift is a result of structural changes in the electrode material during discharge.

4.3. EXAFS

EXAFS spectra were recorded during discharge of the cell at beamline 2.3 at SSRL. Fig. 5 shows the k -weighted EXAFS oscillations $\chi(k)$ of the absorption curve when the average Mn oxidation state was 3.39. For this single figure we have used the computer program *EXAFS pour le Mac* (Michalowicz, 1991, 1997) for the pre-edge fit and baseline fit, determination of absorption edge and removal of monochromator glitches. All other EXAFS data were analyzed using the computer program *EXAFSPAK* (George *et al.*, 2000).

The evolution of the Fourier transform (FT) amplitudes of six scans during the entire discharge process is displayed in Fig. 6. In both scans we assigned the manganese oxidation states, derived from the chemical shift of the XANES spectra (as exercised in §4.1). The deepest state of discharge obtained in this particular experiment corresponds to an average manganese oxidation state of +3.09, and to a nominal stoichiometry $\text{Li}_{1.82}\text{Mn}_2\text{O}_4$.

Since these data have not been corrected for the phase shift, distances are given in terms of $R + \Delta R$. The peak at 1.92 Å corresponds to the Mn–O distance, and the peak at 2.82 Å corresponds to the Mn–Mn distance.

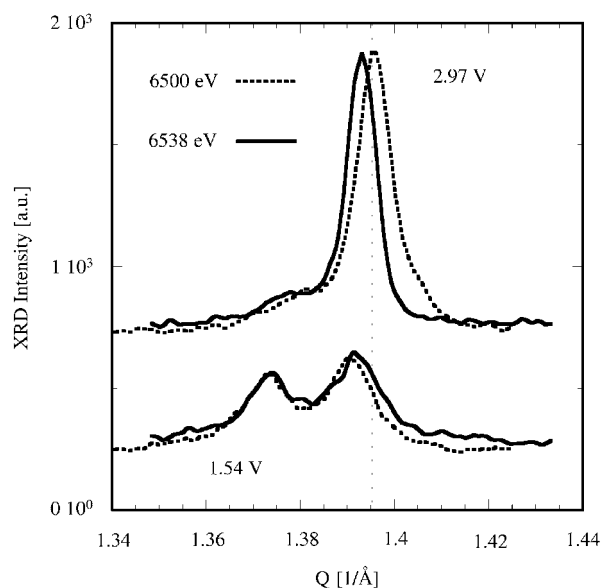


Figure 4
[111] Bragg reflection in the uncharged (single peak) and deeply discharged (split peak) state for energies at 6538 eV (solid line) and 6500 eV (dotted line).

We first notice that, upon discharging, the intensity of the peaks decreases systematically. The reverse effect, *i.e.* increasing peak heights upon charging, has already been reported (Nakai *et al.*, 1999; Shiraishi *et al.*, 1997) and attributed to structural ordering of MnO_6 octahedra when manganese approaches a uniform valence state of Mn^{+4} . The extension of this interpretation for the discharge process is obviously not applicable. This is not surprising because the manganese is being reduced during discharge from an average oxidation state of $\text{Mn}^{+3.5}$ towards $\text{Mn}^{+3.0}$, and Mn^{+3} is known to be the high-spin Jahn–Teller ion of manganese with a pronounced tetragonal distortion of either MnO_6 octahedra.

Then, we notice that the peak for the Mn–Mn distance experiences a gradual shift from 2.82 to 2.74 Å during discharge. In the inset in Fig. 6 the FT amplitudes were divided by a constant factor such that the peak for the Mn–O distance is normalized to unity. The range from 1 to 3.5 Å is magnified to show how the peak for the Mn–Mn distance shifts. The normalization also makes clear that the small peak at 3.35 Å is systematically shifted towards 3.16 Å, increasing in intensity, at the cost of intensity of the peak at 2.82 Å (2.74 Å, respectively).

It is remarkable, however, that the Mn–O distance at 1.92 Å turns out to be very robust *versus* discharging, since this peak experiences no shift at all.

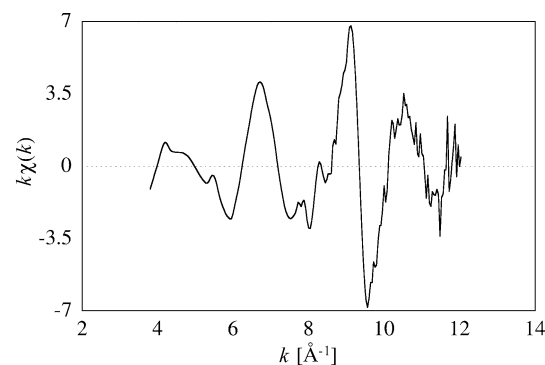


Figure 5
EXAFS $k\chi(k)$ of the sample while Mn was in the oxidation state of 3.39.

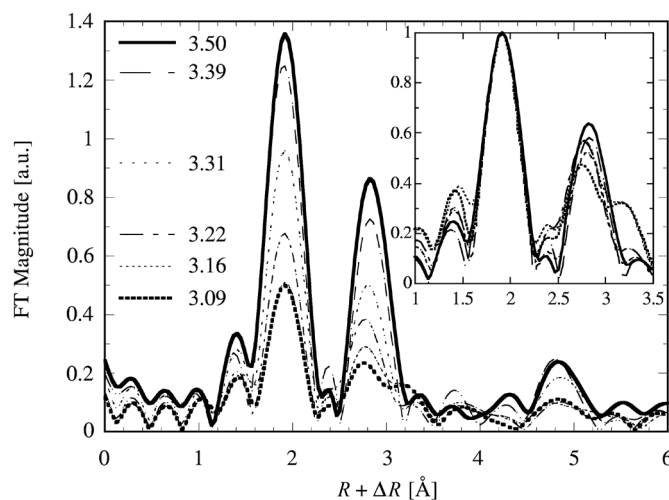


Figure 6
Evolution of EXAFS Fourier magnitude for Mn during discharging from average Mn valence 3.5 to 3.09. Magnified inset with FT maxima normalized to unity.

4.4. ASAXS

Small-angle X-ray scattering (SAXS) is used to study the structure of disordered media on a nanoscale, resolving structures with sizes ranging from 1 nm to fractions of a μm .

SAXS can be considered as diffuse scattering of monochromatic X-rays with respect to the (000) Bragg reflex. By convention, small-angle scattering occurs between the angle of specular beam and the half angle of the first Bragg reflex position. SAXS, and small-angle neutron scattering, have already been used for *ex situ* microstructure analyses of glassy carbon electrodes, such as in electrochemical capacitors (Braun *et al.*, 1999, 2003).

Anomalous small-angle X-ray scattering (ASAXS) is small-angle scattering with at least two different X-ray energies. Scattering curves (SCs) are obtained with an X-ray energy before the absorption edge of a particular element, and right after the absorption edge. This technique is called contrast variation and allows the separation of the scattering contribution from objects containing a particular chemical component from other contributions (Fratzl *et al.*, 1992).

Battery electrodes are relatively complex in terms of microstructure and chemical composition. They contain carbon, active material such as the spinel, and also pores and electrolyte. The X-ray SC obtained by an *in situ* experiment contains structural information of the electrode, but also of the cell parts.

With SAXS at one single X-ray energy only, no unambiguous distinction can be made between either phases. Tuning the X-ray energy to the manganese *K*-edge, however, and subtracting the SC taken before the absorption edge of manganese from the SC taken at the absorption edge, yields an SC which contains information about the manganese-rich structures only.

ASAXS was carried out at the Advanced Photon Source (APS, BESSRC-CAT) for a period of 40 h, during which the cell was slowly charged to 4.3 V, and thereafter discharged back to 3.05 V.

Sets of SCs were sequentially recorded at 20 different X-ray energies between 6350 and 6550 eV near the manganese *K*-shell absorption edge to allow for contrast variation due to the anomalous scattering of the Mn. Owing to the thin design of the *in situ* cell with beryllium X-ray windows, a single SC could be acquired in only 0.1 s, and the overall acquisition time for a set of 20 SCs was only 1 min. Therefore the ASAXS studies can be considered as a time-resolved experiment. About 60 sets of such 20 SC were recorded during the entire experiment. The SCs at energies of 6400 and 6545 eV were chosen for further data analysis (Braun *et al.*, 2001).

Fig. 7 displays SCs of the entire cell, obtained at four different X-ray energies prior to any charging of the electrode in the cell. The corresponding energies are noted accordingly in the plot. Intensity changes among either four SCs as functions of the X-ray energy are due to X-ray fluorescence and anomalous scattering of the manganese. By appropriate subtraction algorithms (Fratzl *et al.*, 1992; Braun *et al.*, 2001), the scattering of the Mn-containing objects can be obtained.

The inset in Fig. 7 shows one SC of the discharged cell. This curve was analyzed for anomalous scattering as described by Fratzl *et al.* (1992) and fitted with two Guinier functions (Braun *et al.*, 2001). This SC represents structural data of the Mn in the electrode only. All other contributions, such as from the cell parts, carbon and pores, are subtracted.

Fig. 8 shows the SC of the manganese in the electrode in its uncharged, charged and discharged state. The humps in the data curves account for the presence of structural inhomogeneities, such as nanocrystallites or aggregates or agglomerates. They can be approximated by Guinier functions and analyzed quantitatively. The

data points are the actual data, and the drawn lines are sums of two Guinier functions for the charged and discharged electrode. For the uncharged electrode we found that three Guinier ranges were present. For further details of the ASAXS experiment and interpretation of the data, we refer the reader to Braun *et al.* (2001).

5. Summary

A versatile and easy to manufacture, easy to assemble, re-usable electrochemical *in situ* battery cell for X-ray experiments in transmission was tested with LiMn_2O_4 -based electrode material at various synchrotron beamlines. The cell contains a lithium metal counter electrode and can operate safely for more than 40 h without significant traces of corrosion. The thin cell design with beryllium X-ray windows permits a high transmission for quality data on the chemical shift, crystallographic phase transitions and changes of the microstructure during electrochemical reaction.

Financial support by the US Department of Energy and by the DOE Office of Basic Energy Sciences, Contract No. DE-AC03-76SF00098 is gratefully acknowledged. SSRL and APS are national user facilities operated by Stanford University and the University of

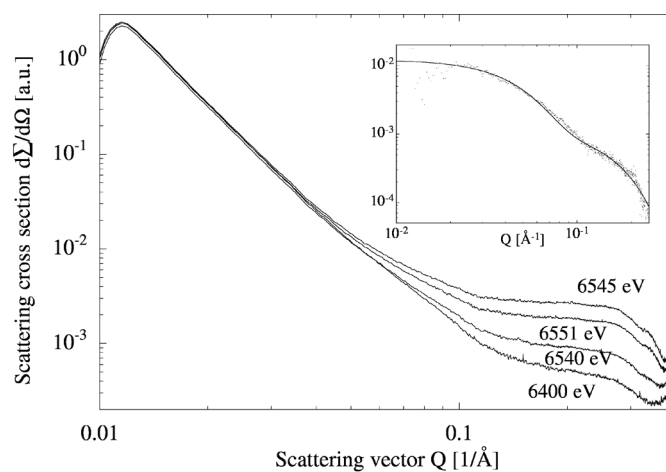


Figure 7 Scattering curves of the entire *in situ* cell, obtained at four different X-ray energies.

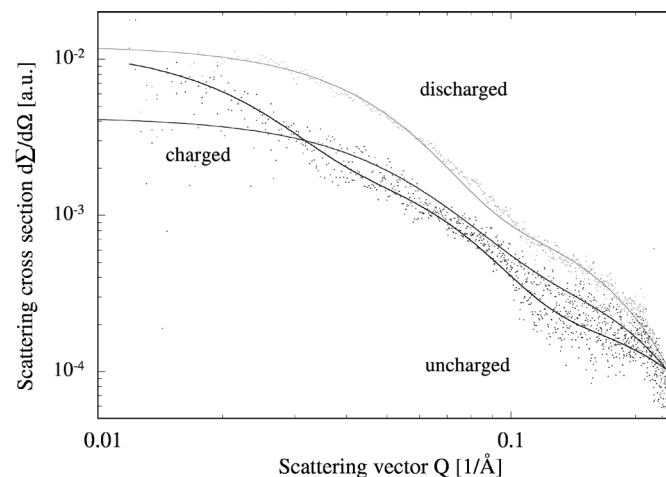


Figure 8 Scattering curves of manganese oxide in electrode matrix for three different states of charge.

Chicago, respectively, on behalf of the US Department of Energy, Office of Basic Energy Sciences. BAO and ACF gratefully acknowledge financial support from the US Department of Energy summer internship programs (PST, ERULF). Helpful discussions with Dr Otto Haas (Paul Scherrer Institut, Villigen, Switzerland), with Dr Craig R. Horne (Nanogram Corporation, Fremont, California, USA), and technical assistance from the machine shop, UCB College of Chemical Engineering, are gratefully acknowledged.

References

- Balasubramanian, M., Sun, X., Yang, X. Q. & McBreen, J. (2001). *J. Power Sources*, **92**, 1–8.
- Braun, A., Bärtsch, M., Schnyder, B., Kötz R., Haas, O., Haubold, H.-G. & Goerigk, G. (1999). *J. Non-Cryst. Solids*, **260**, 1–14.
- Braun, A., Kohlbrecher, J., Bärtsch, M., Schnyder, B., Kötz, R., Haas, O. & Wokaun, A. (2003). *Electrochim. Acta*. To be submitted.
- Braun, A., Seifert, S., Pappannan, T., Cramer, S. P. & Cairns, E. C. (2001). *Electrochem. Commun.* **3**, 136–141.
- Dunitz, J. D. & Orgel, L. E. (1957). *J. Phys. Chem. Solids*, **3**, 20–29.
- Fratzl, P., Yoshida, Y., Vogl, G. & Haubold, H.-G. (1992). *Phys. Rev. B*, **46**, 13323–13331.
- George, G., George, S. & Pickering, I. (2001). *EXAFSPAK. A Suite of Computer Programs for Analysis of X-ray Absorption Spectra*, <http://www-ssl.slac.stanford.edu>.
- Gérard, B., Blyr, A., Du Pasquier, A., Leriche, J. B., Seguin, L. (1999). *J. Power Sources*, **81/82**, 922–924.
- Kanno, R., Kondo, A., Yonemura, M., Gover, R., Kawamoto, Y., Tabuchi, M., Kamiyama, T., Izumi, F., Masquelier, C. & Rousse, G. (1999). *J. Power Sources*, **81/82**, 542–546.
- Koetschau, I., Richard, M. N., Dahn, J. R., Soupart, J. B. & Rousche, J. C. (1995). *J. Electrochem. Soc.* **142**, 2906–2910.
- Michalowicz, A. (1991). *EXAFS pour le MAC*, in *Logiciels pour la Chimie*, pp. 102–103. Paris: Société Française de Chimie.
- Michalowicz, A. (1997). *J. Phys. IV*, **7**, C2–235.
- Mishra, S. K. & Ceder, G. (1999). *Phys. Rev. B*, **59**, 6120–6130.
- Nakai, I., Shiraishi, Y. & Nishikawa, F. (1999). *Spectrochim. Acta*, **B54**, 143–149.
- Richard, M. N., Koetschau, I. & Dahn, J. R. (1997). *J. Electrochem. Soc.* **144**, 554–558.
- Ronci, F., Scrosati, B., Rossi Albertini, V. & Perfetti, P. (2001). *J. Phys. Chem. B*, **105**, 754–759.
- Shiraishi, Y., Nakai, I., Tsubata, T., Himeda, T. & Nishikawa, F. (1997). *J. Solid State Chem.* **133**, 587–590.
- Yamada, A., Tanaka, M., Tanaka, K. & Sekai, K. (1999). *J. Power Sources*, **81/82**, 73–78.